Innovative and bench-tested numerical demonstrator for hybrid electric propulsion design

Dr. Jessica NEUFOND, Vibratec, Ecully, France
Adrien PARPINEL, Vibratec, Ecully, France
Lionel DUVERMY, Vibratec, Ecully, France

Abstract

As part of the CORAC technological roadmap, the TURBOLAB project investigates the design and modelling of hybrid turboprop systems. The integration of an electric engine and a gearbox on a shaft line is a complex task, as both components generate dynamic loads that must be fully understood to ensure shaft line integrity. Building on previous work analyzing test rig results, this paper presents the numerical models developed within the TURBOLAB R&T project to predict the torsional behavior of a geared shaft line integrating an electric motor. The numerical demonstrator provides access to the torsional response of the complete shaft line under electromagnetic and gear mesh excitations. Each modelling step is validated through correlation with experimental data from the physical test rig. This work advances the state of the art by bridging two historically distinct domains—electric motor dynamics and gear transmission behavior—and proposes a unified, predictive modelling approach from the early design stages.

1. INTRODUCTION

As part of the Civilian Aviation Research Council (CORAC) technological roadmap, the Research & Technology (R&T) TURBOLAB project contributes to the energy and competitiveness revolution.

Figure 1: CORAC and TURBOLAB logos

Preliminary to industrial applications, the project is related to other CORAC framework programs:

- Program DOPEE run by SAFRAN Aircraft Engines with technical aims to investigate electrical engine integration in turbofan architecture and build a demonstrator on a 1:1 scale.
- Hybrid turboprop program run by SAFRAN Helicopter Engines with aims to develop a new turboprop.

The hybridization of aircraft and rotorcraft propulsion systems has regained significant interest in recent years, driven by global efforts to reduce greenhouse gas emissions. While the automotive industry has already capitalized on hybrid and fully electric propulsion technologies, the aeronautical sector faces distinct technical challenges in safely integrating electric engines into flight systems. These challenges stem from the stringent safety, reliability, and performance requirements specific to aerospace applications.

The dynamic behavior of electric engines is well documented, with electromagnetic pressures in the airgap being predictable and commonly used to assess structural vibrations, as demonstrated by Dupont et al. (Ref. 1). Similarly, gearboxes are known to introduce complex dynamic excitations, adding further challenges to the torsional behavior of shaft lines, as analyzed by Neufond (Ref. 2). Gear dynamics, primarily driven by the meshing process (Ref. 3, Ref. 4), have been extensively studied. Both electromagnetic and gear mesh excitations can induce structural vibrations and torque ripple, potentially exciting torsional modes of the shaft line. While the literature provides substantial insights into each of these phenomena independently, recent studies addressing their combined effects remain limited. Van Binsbergen et al. (Ref. 5) proposed a multi-body simulation to assess generator torque ripple in a wind turbine drivetrain, yet without a detailed analysis of the respective contributions from electric motors and gearboxes. This highlights a remaining gap in the literature.

The developments and results discussed in this paper enhance the state of the art by proposing an innovative and efficient approach to predict the risks involved in integrating an electric motor onto a geared propulsion shaft line. Originating from the

TURBOLAB R&T project, this work brings together two historically distinct fields of expertise: electric motor dynamics (Ref. 1) and gear system dynamics (Ref. 2, Ref. 6). One of the key challenges lies in predicting, from the early design stages, the torsional behavior induced by the combined excitations of these two systems. For this purpose, a dynamic test rig, shown in Figure 2, was designed to replicate the dynamic effects at stake in a controlled environment. Therefore, each modelling step can be systematically validated through correlation with experimental data obtained from the physical test rig, as a follow-up of the previous paper dedicated on test rig demonstrator (Ref. 7).

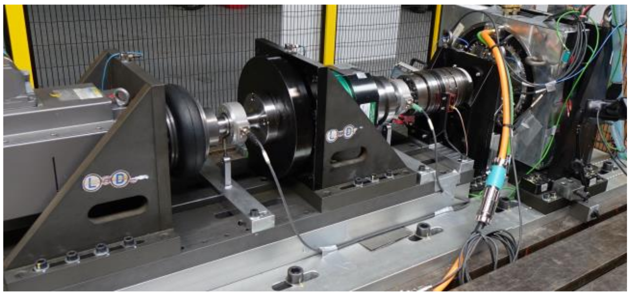

Figure 2: Picture of TURBOLAB test rig at Vibratec

2. NUMERICAL DEMONSTRATOR

2.1. General overview

To support early-stage design decisions and assess the dynamic behavior of hybrid shaft lines, a dedicated numerical demonstrator is proposed. This tool aims to replicate the physical phenomena observed on the test rig while offering flexibility for parametric exploration. Particular attention has been given to ensuring full control over the modelling environment. The proposed approach enables efficient parametric studies while minimizing computational time. The complete process used to compute the shaft line's dynamic response is illustrated in Figure 4. In this context, the dynamic response refers to the torque fluctuations along the shaft line. One of the key strengths of the methodology lies in the use of a unified Finite Element Model (FEM) framework, capable of incorporating both gear mesh and electromagnetic excitations. Based on the assumption of weak coupling between these two sources, the excitations can be computed independently and subsequently projected onto the structural model.

The proposed paper gives a general overview of the electromagnetic and gear mesh loads computation and their projection onto the hybrid shaft line model. As part of this project, it is necessary to perform reverse engineering, a review of which is presented in this article. Indeed, reliable prediction of electromagnetic and meshing forces requires in-depth knowledge of the machine's parameters. Comparing calculations with measurements ensures confidence in the results before projecting them onto the complete hybrid shaft line model.

2.2. Application on TURBOLAB test-rig demonstrator

To ensure consistency between experimental and numerical investigations, the same 3D Finite Element Model (FEM) of the shaft line was used both for the design of the test rig (Ref. 1) and for the numerical demonstrator. The test rig is built to test:

- Electric engine: synchronous permanent magnet motor 66 poles, 72 slots, 700N.m max torque, 600rpm max speed,
- Gearbox: single stage epicyclic gear set, spur gears, 3 planets, ratio 4, up to 400N.m,

This model focuses specifically on the torsional behavior of the shaft line and relies on a set of simplifying assumptions, including concentrated masses, lumped inertias, and equivalent rotational stiffnesses. An overview of the FEM architecture is provided in Figure 3.

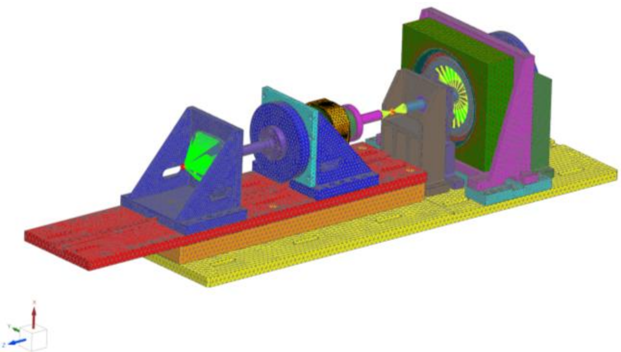

Figure 3: FEM models of the test bench

Among the objectives of the TURBOLAB project was the design of a shaft line with its first torsional mode below 50 Hz. This requirement was successfully met during the test rig development, with the first torsional eigenfrequency set at 42.5 Hz. The same Finite Element Model (FEM) used for the numerical demonstrator was employed during the design phase to predict the dynamic behavior of the shaft line. A comparison between the computed and measured

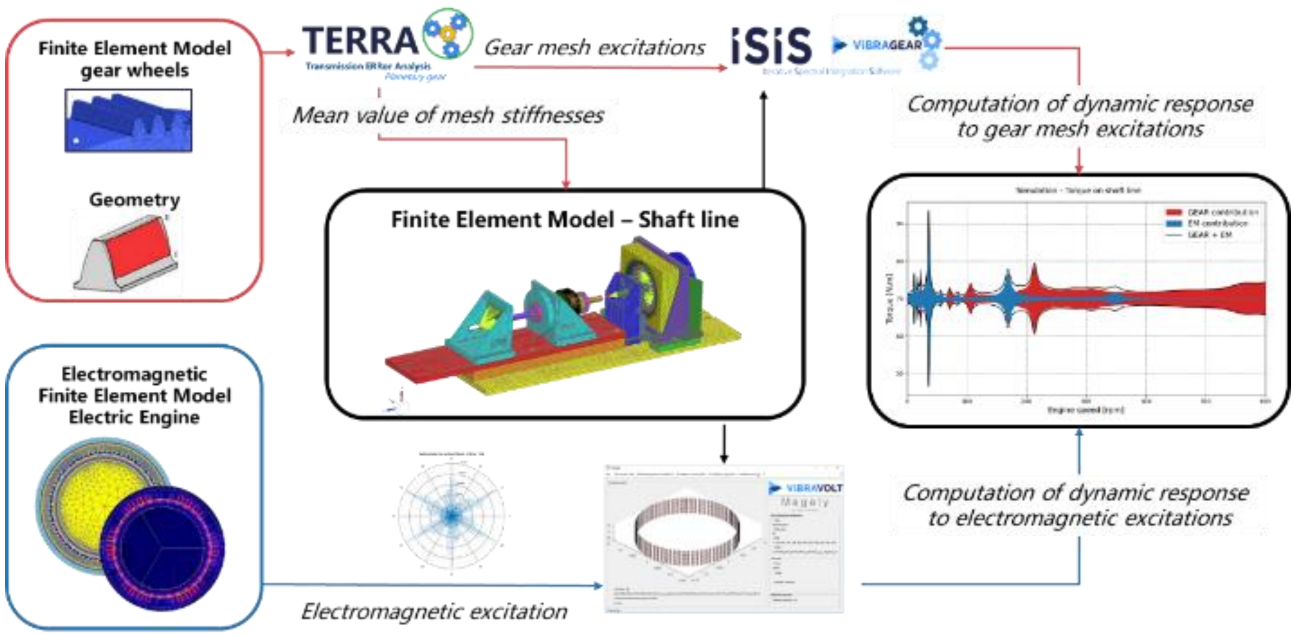

Figure 4: Numerical demonstrator process for shaft line response to dynamic excitations.

eigenfrequencies is provided in Table 1, confirming the model's ability to accurately capture the system's torsional characteristics.

Table 1: Shaft line first modes

Shaft line mode	Model	Test rig	deviation
1st torsion	39.9Hz	42.5Hz	-6%
1st bending	112.0Hz	125.6Hz	-11%
2nd torsion	180.5Hz	184.5Hz	-2%
3rd torsion	385Hz	405Hz	-5%

3. ELECTROMAGNETIC AND GEAR MESH LOADS MODELS

This chapter focuses on the validation of the electromagnetic and gear mesh excitation models prior to their application on the common structural framework. The objective is to ensure that each excitation source is accurately characterized before being projected onto the shared Finite Element Model (FEM) of the shaft line, which is addressed in the following chapter.

3.1. Electromagnetic model

In the case of electric motors, the primary source of excitation is the Maxwell pressure. Simulations including magnetostriction effects in the magnetic circuit have shown that this phenomenon does not significantly contribute to vibration generation. Similarly, Lorentz forces are negligible for this type of motor and can be disregarded.

Maxwell pressures arise at the interface between two media with different magnetic permeabilities (μ), in the presence of a magnetic field. In electric machines, these pressures act on the rotor and stator surfaces adjacent to the airgap. Their dynamic nature is responsible for exciting structural vibrations. The radial and tangential components of the Maxwell pressure are expressed as:

$$P_r = \frac{1}{2\mu_0}\left(B_r^2 - B_t^2\right) \qquad (1)$$

$$P_t = \frac{1}{\mu_0}\left(B_r B_t\right) \qquad (2)$$

Where B_r and B_t are the radial and tangential components of the magnetic flux density, and μ_0 is the permeability of free space.

The radial component is typically the main contributor to stator vibrations and subsequent acoustic radiation. The tangential component also contributes to stator vibrations and induces torque ripple through its reciprocal action on the rotor, which can propagate through the drivetrain, potentially leading to vibratory issues and system failures.

The electromagnetic model is built using Altair Flux™ and solved in the time domain. A magneto-transient simulation is performed to compute the evolution of the magnetic field distribution and torque during rotor rotation, under constant speed and imposed current conditions. This modelling approach allows for a detailed analysis of the sensitivity of electromagnetic excitations to machine topology. Figure 5 gives an overview of the electric engine electromagnetic model.

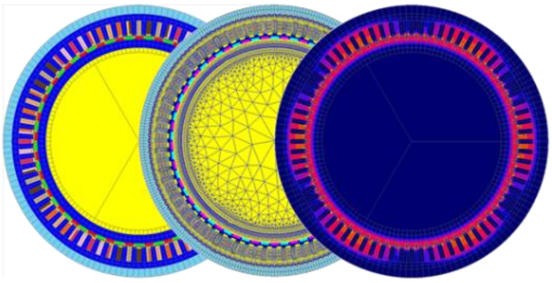

Figure 5: Electromagnetic modelling of electric engine geometry (left), mesh (middle), example of result (right)

A big challenge for this R&T project was to setup such model, without any information from supplier. Reverse engineering was inevitable to achieve this work. This relies on experimental data, including measured torque harmonics, electric engine supply currents and electromagnetic unbalance.

3.2. Electromagnetic unbalance calibration and parameter sensitivity analysis

Due to limited access to proprietary motor data, several assumptions were necessary. In particular, the exact magnetic properties of the laminated steel sheets used in the rotor and stator could not be identified (see Figure 6 for photo of the electric engine sheet metal stack taken during reverse engineering). As a result, default ferromagnetic materials from the Altair Flux™ database were used.

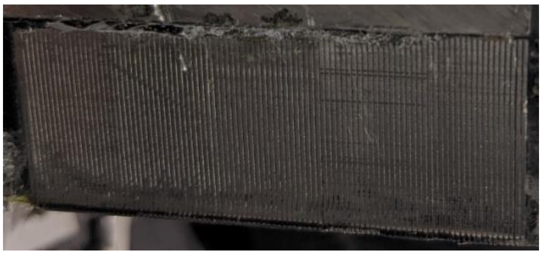

Figure 6: Photo of the electric engine sheet metal stack taken during reverse engineering

Another reverse engineering work performed was to confirm the value of the residual induction of the magnets to be implemented in the model. For this purpose, numerical checks were carried out using the electromagnetic model. The maximum power operating point is selected; the technical documentation indicates that the motor delivers 710N.m of torque at a maximum current of 106 Arms. The objective is then to compare the simulated electromagnetic torque at different values of $\boldsymbol{B_r}$ (remanent induction of the magnets) to approximate the technical data of the motor. The values obtained are reported in the Table 2.

Table 2: Average torque simulated for different values of residual induction $\boldsymbol{B_r}$ of the magnets, under maximum current of 106 Arms

$\boldsymbol{B_r}$ [T]	Mean torque [N.m]
0.9	559
1.00	620.7
1.05	651.4
1.10	682.0
1.15	712.6

One of the main objectives of the project is to predict the electromagnetic unbalance, which requires accurate modelling of the machine's internal forces. Indeed, in some cases, this electromagnetic unbalance can lead to greater amplitude than mechanical unbalance. A correlation between the calculated unbalance and rotor dynamic eccentricity was established and is illustrated in Figure 7. The numerical model confirms the linear trend observed in experimental data but tends to overestimate the unbalance.

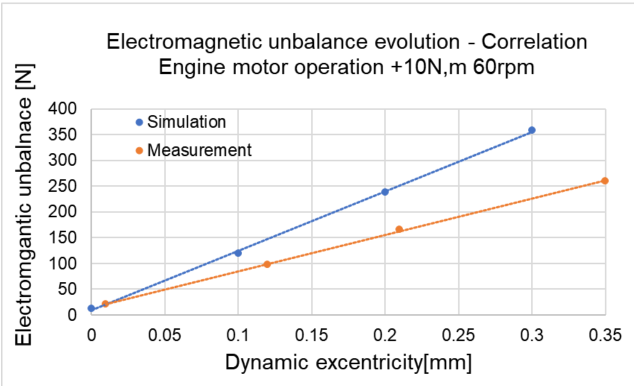

Figure 7: Correlation between the evolution of electromagnetic unbalance at the operating point electric engine motor +10N.m 60rpm

To better understand this discrepancy, a sensitivity analysis was conducted using the Morris method. The goal was to identify the most influential parameters affecting the unbalance calculation and to quantify the impact of modelling uncertainties. Figure 8 gives an overview of results obtains, with highlighting of parameters uncertainties on electromagnetic imbalance level.

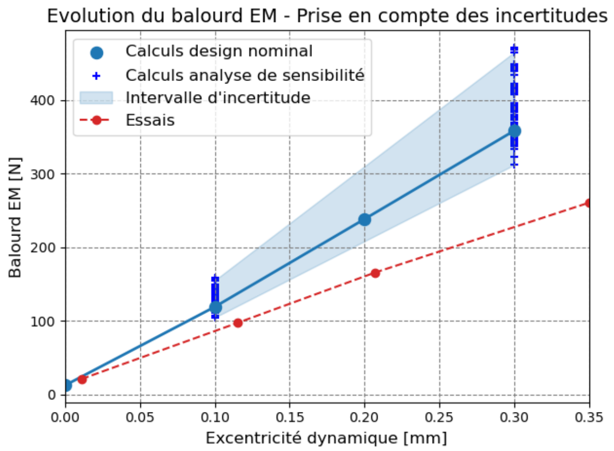

Figure 8: Evolution of electromagnetic unbalance considering uncertainties, correlation with tests, electric engine motor operating point +10N.m 60rpm

This analysis highlights the strong influence of input parameter variability and the inherent difficulty of accurately predicting electromagnetic unbalance without detailed knowledge of the motor's internal characteristics.

3.3. Gear mesh load modeling

Integrating a gearbox into the shaft line affects both the mechanical and dynamic behavior of the system. It introduces an equivalent torsional stiffness and acts as a source of excitations, mainly due to transmission error and mesh stiffness variations (see Ref. 3). Nonlinear effects like vibro-impact between teeth are beyond the scope of this work, but whining noise remains intrinsic to gear systems. In the TURBOLAB project, the focus is on torsional excitations from the gearbox and their interaction with the electric motor.

Assuming perfectly rigid and ideal gears, the involute tooth profile ensures a constant transmission ratio. In practice, however, geometric imperfections, profile corrections, and elastic deformations of drivetrain components cause fluctuations in the instantaneous ratio. This results in a deviation between the actual and theoretical output shaft positions, known as Transmission Error (TE), a parametric internal excitation.

Using Willis' equation, the global TE Δ (in meters) between the sun gear and the carrier in a planetary gear set (type I) can be expressed as:

$$\Delta = R_{bs}\theta_{s/0} - (R_{bs} + R_{br})\theta_{c/0} \tag{3}$$

With R_{bs} and R_{br} the base radii of sun gear and ring gear, respectively, $\theta_{s/0}$ and $\theta_{c/0}$ the rotational angle of sun gear and ring gear, respectively.

Under load, elastic deformations of gear teeth cause a periodic variation in tooth approach, modeled by a local meshing stiffness:

$$k_j(\theta) = \frac{\partial F_j}{\partial \delta_j}(\theta) \tag{4}$$

This periodic stiffness acts as a parametric excitation source, potentially leading to dynamic instabilities.

The epicyclic gearbox is modeled using a structural FEM combined with the TERRA module of the VIBRAGEAR software to compute internal meshing excitations (see Figure 9). Close collaboration with the supplier provided full access to system data, ensuring accurate representation.

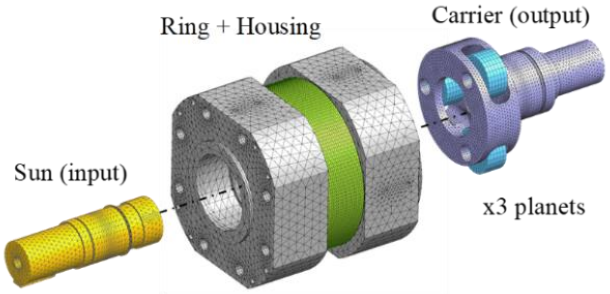

Figure 9: Gearbox FEM model

This work contributed to the development of the latest VIBRAGEAR version. Additionally, the frequency-domain approach implemented in VIBRAGEAR enables significantly reduced computation times compared to time integration, making parametric studies feasible.

3.4. Correlation of Static Transmission Error (STE) with measurement

The validation of STE calculations for epicyclic gear trains is based on a comparison between simulation results and experimental measurements (see Ref. 7 for more detailed about measurement process).

Tests conducted on the TURBOLAB test-rig covered multiple operating configurations, including variations in electric engine operating mode (motor or generator) and applied torque levels. Correlation is performed at 60rpm (electric engine) to ensure no coincidence between mesh harmonic and shaft-line mode. For such epicyclic gear set, only the overall transmission error can be accessed in measurement. Therefore, gear model validation is performed regarding the overall STE. The correlation results between simulated and measured peak-to-peak STE for both motor and generator operating modes, across the different load cases tested, are presented in Figure 10.

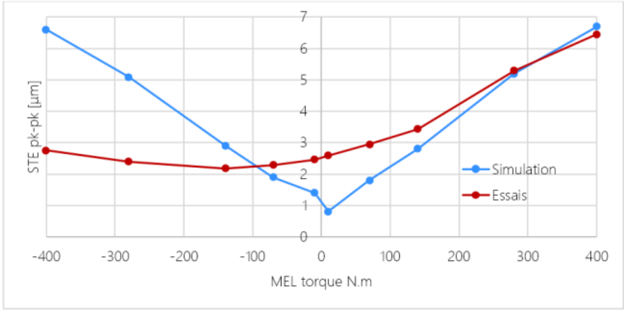

Figure 10: Correlation of peak-to-peak transmission error

In motor operating mode, simulations successfully capture the STE, particularly under high load. In generator mode, however, the correlation is less consistent. While simulations show only minor differences between operating modes, measurements reveal an opposite trend: a relatively stable peak-to-peak STE is observed with increasing load in generator mode. It should be noted that optical encoders are not mounted directly on the gearbox input and output shafts, but on an intermediate component assumed to be rigid. A slight slip at this interface during testing cannot be ruled out and may affect measurement accuracy.

Nevertheless, the overall agreement between simulation and measurement provides enough confidence in the qualitative and quantitative accuracy of the numerical model.

4. GEAR MESH AND ELECTROMAGNETIC EXCITATIONS PROJECTION IN THE HYBRID SHAFT LINE MODEL

The numerical demonstrator is applied to the case of a constant load on the electric engine, operating in motor mode at +70 N.m, during a speed ramp up to 600 rpm. The validation of the numerical demonstrator follows the same approach as previously described, relying on comparison between simulation and experimental measurements.

4.1. Dynamic Transmission Error (DTE)

Fluctuations in static transmission error (STE) and local meshing stiffness are implemented in the dynamic model as parametric excitation sources acting on the kinematic response of the epicyclic gear train. As STE refers to mesh excitations at quasi-static state, DTE refers to mesh excitations under dynamic amplification induced by working condition (speed) and system response

The method is based first on introducing elastic coupling between teeth through the average values of meshing stiffness, linearized around the static load conditions, and on determining the system's modal basis, derived from the finite element discretization of all epicyclic gear train components (gears, bearings, housing, etc.).

Assuming the system is linearized around its equilibrium position, the equation of motion to be solved is expressed as:

$$\mathbf{M_{EF}}\ddot{x} + \mathbf{C}\dot{x} + \left(\mathbf{K_{EF}} + \sum_{j=1}^{2N} k_j\,(t) R_j R_j^T\right) x = \sum_{j=1}^{2N} k_j\,(t) R_j R_j^T x_s \qquad (5)$$

ISIS software is designed to compute the dynamic displacement response of one or several nodes. In particular, the FEM model is built to provide access to the rotational response of the input and output shaft nodes. Figure 11 provides an overview of ISIS main inputs and ouputs.

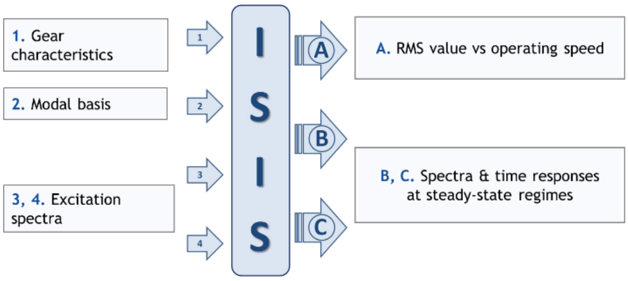

Figure 11: ISIS software principle

In preparation for simulations and post-processing, nodes are defined along the axis of rotation at the input and output of the gearbox. The shafts are simplified to a 1D representation, as illustrated in Figure 12.

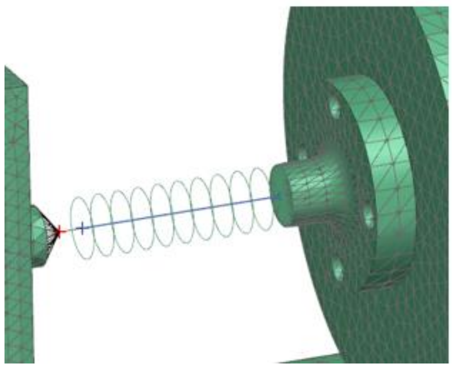

Figure 12: 1D finite element modeling of the input and output shafts of the gearbox

The validation of DTE calculations is based on a comparison with test results. As a reminder, the numerical demonstrator is deployed in the case of a constant electric engine load, in engine mode, around +70N.m, for an electric engine speed increase up to 600rpm. These operating conditions correspond to tests 44 and 66, recorded separately during the measurement campaign. They are assumed to be strictly identical.

A certain degree of caution is required regarding the correlation between calculations and measurements in this type of test. It should be noted that DTE post-processing is very sensitive to speed variability, especially at low speed. Consequently, the post-processing of the DTE is coarse, due to insufficient speed stabilization. At higher speeds, the post-processing tends towards the conditions required for TE measurement. Nevertheless, their analysis provides valuable insight, highlighting the repeatability or dispersion of the results.

Results are given Figure 13.The field of uncertainty associated with the measurement, defined from the two available tests, is shown, as well as that relating to the simulation. As a reminder, the position of the encoders is estimated from the CAD of the test bench, although there is a slight difference with the real position cannot be excluded.

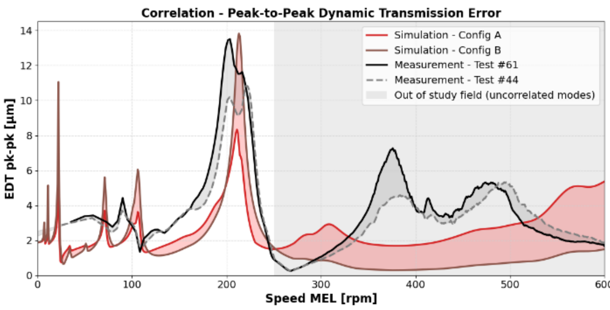

Figure 13: Correlation of overall peak-to-peak DTE. Measurements and simulations. Run-up electric engine +70N.m

The experimental results show that critical speed ranges are clearly identified. In simulation, the dispersion is more pronounced but correctly captures the main critical speed, located around 220 rpm. Correlation at lower speeds is less straightforward, as the measurement resolution is insufficient to capture dynamic amplifications. Overall, the simulated DTE at the theoretical encoder position tends to underestimate the peak-to-peak amplitude by 2 to 4 µm compared to the measurement. This result is consistent with the correlation observed for the STE at electric engine torque +70 N.m, where a similar underestimation was already noted in simulation.

The global DTE correlation is further supported by the comparison of the first three meshing harmonics, shown in Figure 14. As before, the out-of-scope region is included in the plots. This region extends to lower speeds for the second and third harmonics (H2 and H3), which reduces the correlation in that range. In both simulation and measurement, the first meshing harmonic dominates. Outside dynamic amplification zones, the harmonic hierarchy mirrors that of the STE results. Within the analysis range, dominant peaks are generally well identified. In contrast, the out-of-scope region displays uncorrelated amplifications, likely due to poorly aligned mode shapes.

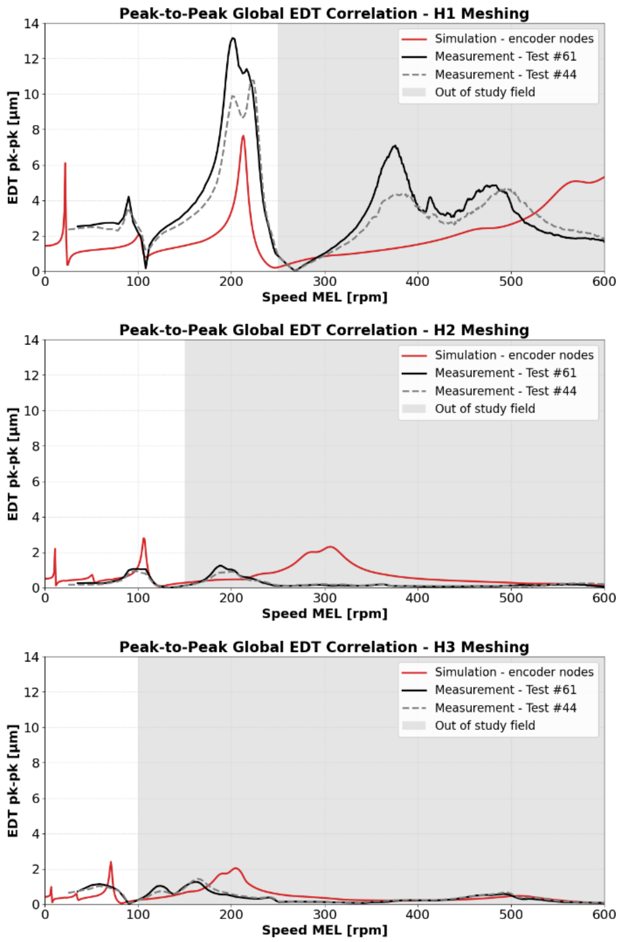

Figure 14: Correlation of the meshing harmonic of peak-to-peak overall DTE. Run-up engine electric engine +70N.m

Confidence in the computed DTE results is supported by a strong history of validation of this modeling approach under steady-state conditions. However, the measurement of DTE during speed ramps - such as those implemented in the TURBOLAB project - remains challenging and does not allow for a fully quantitative correlation of the underlying phenomena. Nevertheless, based on simulation outcomes and prior experience, it remains possible to predict critical operating zones with reasonable confidence, despite the inherent uncertainties in the simulation.

4.2. Torque fluctuation under gear mesh load

Historically, the dynamic behavior of geared transmissions has been primarily studied through the lens of tooth-level interactions and their contribution to radiated noise. In contrast, torque fluctuation is more rarely associated with gearboxes themselves. It is typically regarded as an external excitation - such as engine acyclisme - rather than an intrinsic consequence of the gearbox's dynamic behavior. On this point, the available literature remains limited. This paper proposed an analytical approach compatible with ISIS software.

The torque amplitude as a function of time, $C(t)$, at a given shaft section, can be calculated using the following expression:

$$C(t) = K_{segment} \times \Delta u_{segment}(t) \quad (6)$$

With:

- $K_{segment}$: Torsional stiffness of the shaft segment in N.m/rad,
- $\Delta u_{segment}(t)$: Angular deflection between the two nodes of the shaft segment in rad

To implement the procedure, several segments corresponding to CBEAM elements at the gearbox input or output are considered, as illustrated Figure 15.

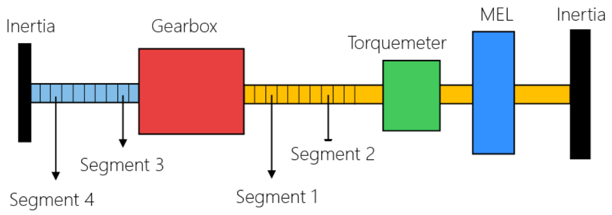

Figure 15: 1D diagram of the shaft line, location of the segments considered at the input and output of the gearbox for calculating the dynamic torque oscillation with the ISIS solver.

Based on Equation 6, the envelope of the torque oscillation amplitude is plotted in Figure 16 for each shaft segment. It should be noted that the mean torque value, set at 70 N.m, is excluded from these simulation results.

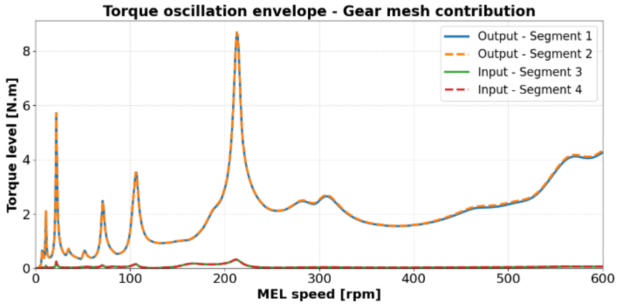

Figure 16: Result of calculation of dynamic torque oscillation at the input and output of the gearbox.

Torque oscillations are nearly identical whether the segment is located at the input or output of the gearbox. This behavior is as expected: if local beam modes are not excited (i.e., at very high frequencies), the dynamic torque oscillation remains uniform along the shaft. However, on either side of a torsional compliant element such as the gearbox, the amplitude of dynamic torque differs. At the gearbox input, the mean torque is theoretically reduced by a factor of 4 due to the reduction ratio. Nevertheless, experimental measurements show a tenfold attenuation of oscillations, highlighting the gearbox's filtering effect.

Within the scope of the project, the focus is specifically on the dynamic oscillation of the torque at the output of the gearbox, i.e. on the torque meter and electric engine side. This dynamic amplification around 70 N.m is shown in Figure 17 (top), with the contributions of the gear harmonics added in Figure 17 (bottom).

The dynamic amplifications correspond to the crossings between meshing excitations and the natural modes of the shaft line. It is worth noting that, although the evolution trend of the computed torque closely follows that of the global DTE, it does not depend on the specific location considered along the output shaft.

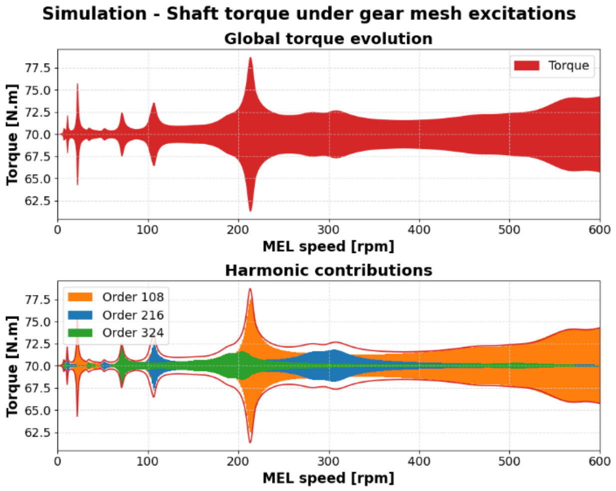

Figure 17: Result of calculation of dynamic torque oscillation at the input and output of the gearbox.

Figure 18 compares the envelopes of dynamic torque oscillations by integrating the first three orders associated with meshing. These oscillations, generated by meshing excitations, are compared with experimental measurements. One limitation of this comparison is the sampling rate of the signals in the tests, and limits the measurement results to approximately 380 rpm.

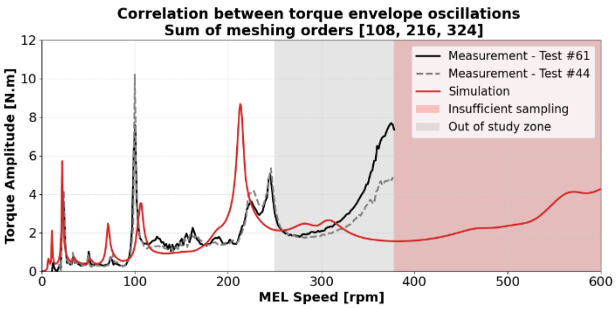

Figure 18: Result of calculation of dynamic torque oscillation at the input and output of the gearbox.

The direct comparison of the envelopes highlights a promising correlation between simulation and measurement. Within the study range, the trend is well captured, and the magnitudes are comparable. The peak-to-peak torque fluctuation around the mean reaches up to ±14% (i.e., 10 N.m oscillation for a 70 N.m mean torque). To better focus the correlation analysis, Figure 19 shows the comparison between simulated and measured torque oscillation amplitudes for each meshing order: 108, 216, and 324.

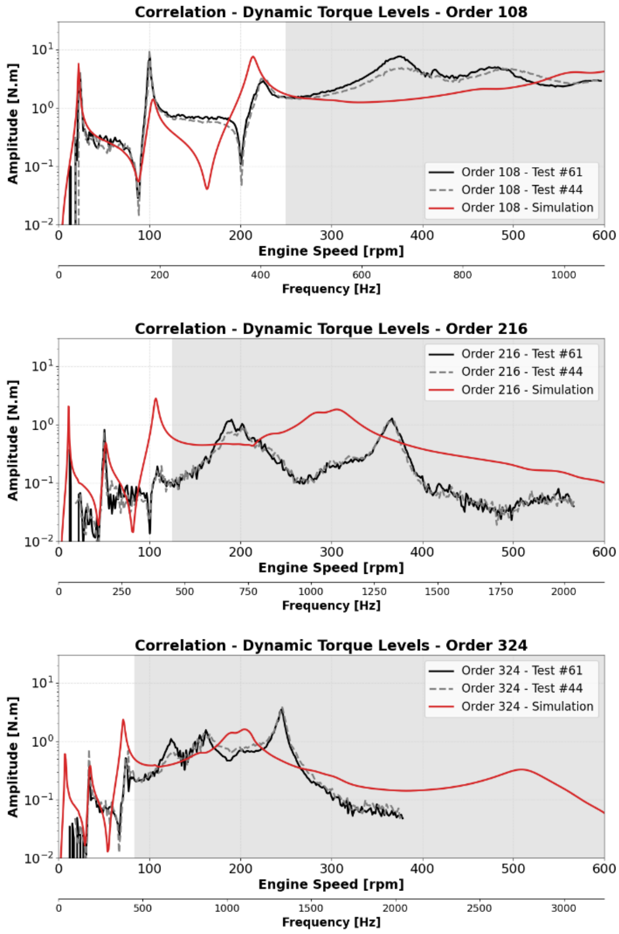

Figure 19: Torque - correlation at meshing order tracking 108, 216 and 324

For the first three orders of meshing, the numerical model correctly predicts the dynamic amplification of torque by exciting the first torsion modes for each order of meshing.

4.3. Electromagnetic torque on run-up

The 2D electromagnetic finite element model (electromagnetic FEM) of the electric motor is used to compute the electromagnetic excitation during the speed ramp. Under constant torque conditions, the variation in electromagnetic excitation throughout the run-up is primarily driven by possible changes in the electric engine supply currents. Based on the tests conducted, the current implemented in the electromagnetic models are updated depending on the electric engine speed, as illustrated in Figure 20.

As shown in Figure 20, a total of 13 electromagnetic calculations were performed to cover the run-up, ranging from 1 to 600 rpm.

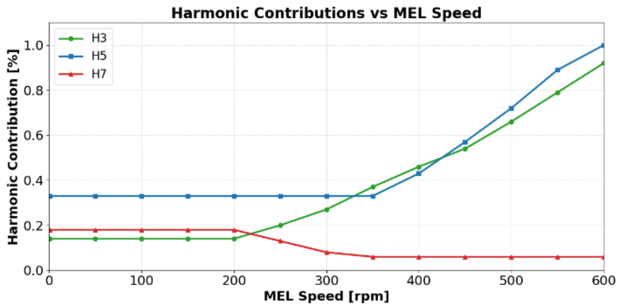

Figure 20: Hamonic contribution in function of electric engine speed

In addition to torque, Maxwell pressures in the airgap are also computed during the speed run-up.

The mechanical mesh used to apply the electromagnetic forces is directly extracted from the full FEM model of the shaft line.

In addition to the mechanical interface, the FEM node representing the geometric center of the electric engine rotor is also included as part of the interface mesh. This node is used as the application point for the electromagnetic excitation on the shaft line.

The VIBRAVOLT software, developed by Vibratec, enables the projection of the electromagnetic excitation onto the mechanical mesh, the interpolation of this excitation over the speed run-up, and the export of the data for order-tracking response calculations. An overview of the VIBRAVOLT interface is shown in Figure 21.

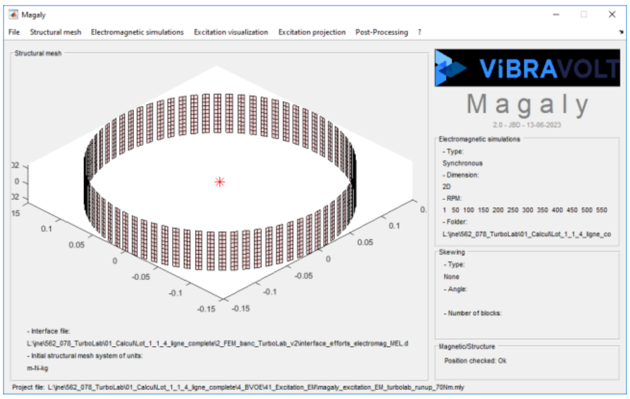

Figure 21: VIBRAVOLT interface

The electromagnetic excitation is provided over the first three orders - 66, 132, and 198 - and interpolated over a speed run-up from 1 to 600 rpm, with a resolution of 1 rpm steps.

4.4. Torque fluctuation induced by electromagnetic load

Final resolution consists of a response calculation by modal superposition. Main assumptions are the following:

- Modal basis computed from 0 to 5 kHz
- Modal damping set to 2% (C/Ccrit)
- Electromagnetic excitations applied at orders 66, 132, and 198

Following the same principle as for gearbox model, the dynamic variation in torque, under the effect of electromagnetic excitation at order 66, is plotted in Figure 22 for each of the nodes at the ends of the CBEAM beam elements modeling the input shaft and output shaft of the gearbox.

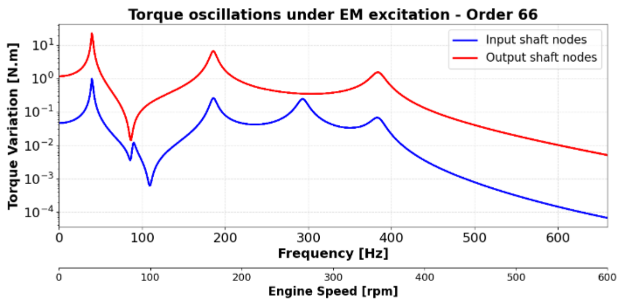

Figure 22: Dynamic torque variations calculated at the nodes of the gearbox output shaft

Two sets of superimposed curves are visible; one characterizes the dynamic torque response of the input shaft (blue curves), the other that of the output shaft (red curves). As with the calculation result for the response to gear meshing excitation, the torque response dynamics are not the same upstream and downstream of the gearbox. Notably, an additional response mode appears at the gearbox input around 285 Hz. This corresponds to a torsional mode specific to the input shaft, which is not observed among the first torsional modes identified at the gearbox output (40 Hz, 180 Hz, and 385 Hz).

The global evolution of torque at the gearbox output is plotted in Figure 23, with the upper graph showing the overall response and the lower graph detailing the evolution of each harmonic contribution.

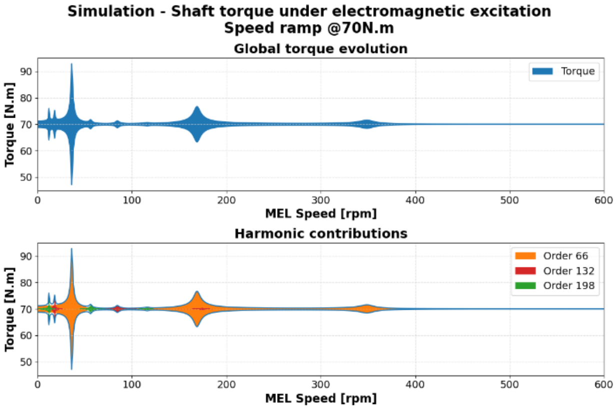

Figure 23: Calculation of the dynamic evolution of torque during acceleration +70N.m, response to electromagnetic excitation only

For each electromagnetic excitation order, three amplification peaks are observed, corresponding to the first three torsional modes of the shaft line. The strongest torque amplification occurs at the crossing between the first excitation order, om66, and the first torsional mode at 40 Hz.

These simulation results are compared with test data. The order-tracking responses for orders 66, 132, and 198 - both computed and measured - are shown respectively in

Figure 24, Figure 25 and Figure 26. In all these figures, frequencies above 450 Hz are considered outside the scope of the present study. For the first three electromagnetic orders, the correlation is particularly satisfactory. The dynamic amplification of the first torsional modes by the electromagnetic excitation is clearly captured across all three orders. The discrepancies between simulation and test data observed beyond 400 Hz are mainly attributed to the lack of model tuning at those frequencies.

This correlation is even more encouraging given that the numerical model relies on several assumptions to compensate for the absence of detailed data on the electric engine.

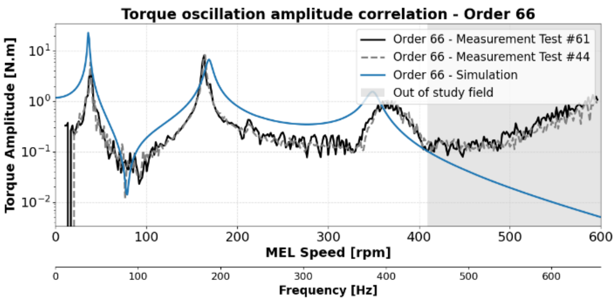

Figure 24: Torque - correlation of order tracking 66

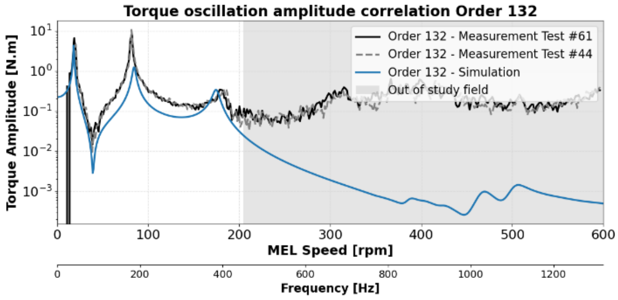

Figure 25: Torque - correlation of order tracking 132

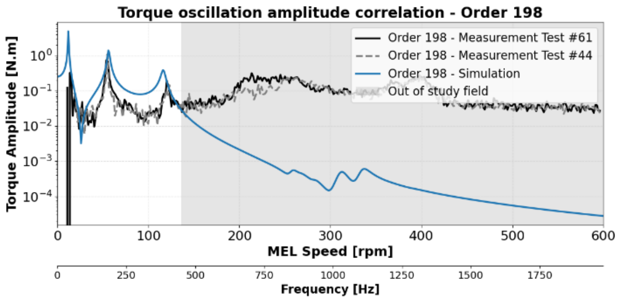

Figure 26: Torque - correlation of order tracking 198

5. OVERALL DYNAMIC RESPONSE OF THE SHAFT LINE

In practice, the dynamic response of the shaft line to gear meshing and electromagnetic excitations is better represented as a superposition of independently computed responses, rather than the result of a fully coupled simulation.

Figure 27 presents an overlay of the previously computed torque results on the gearbox output shaft, in response to both gear meshing and electromagnetic excitations.

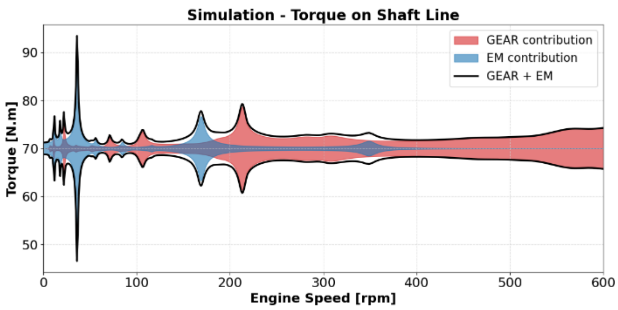

Figure 27: Superimposition of dynamic responses of the drive shaft to meshing and electromagnetic excitations. Run-up, electric engine motor +70N.m

In addition, Figure 28 provides a synthetic view of the correlation between the envelopes of dynamic torque oscillations. For this comparison, the measured signal is reconstructed from the contributions of both electromagnetic and gear meshing excitations (orders 66, 108, 132, 198, 216, and 324).

The figure also includes the computed envelopes corresponding to the responses from gear meshing excitation only and from electromagnetic excitation only.

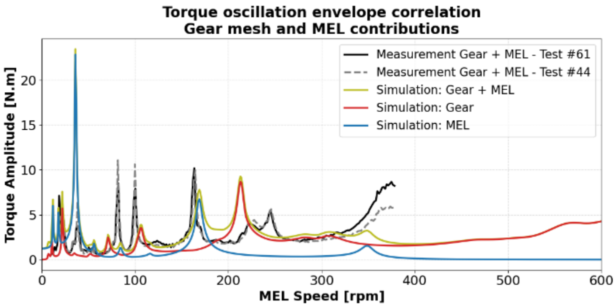

Figure 28: Correlation of the dynamic torque oscillation envelope in response to gear and electromagnetic excitations

In conclusion, the numerical demonstrator enables the prediction of the shaft line's dynamic response to both gear meshing and electromagnetic excitations, particularly at the crossing of the first three torsional modes.

6. CONCLUDING REMARKS AND PESPECTIVES

This work led to the development of a unified numerical demonstrator combining gear dynamics and electromagnetic vibration models, traditionally treated separately. Each model was independently validated using experimental data, confirming their accuracy in replicating physical behavior.

The approach highlighted the strong sensitivity of results to input data quality. The torsional behavior was validated through the first three shaft line modes (40 Hz, 180 Hz, 385 Hz).

Torque fluctuation was the main focus, with a novel contribution being the calculation of torque ripple induced by gear meshing - an aspect few addressed in the literature. Validation during a speed ramp-up under constant torque (70 Nm) confirmed the model's ability to predict resonance crossings linked to both gear meshing (orders 108, 216, 324) and electromagnetic excitations (orders 66, 132, 198).

Nonetheless, current limitations include the absence of gearbox–electric engine coupling and nonlinear effects. Developing a multibody model could enhance physical representativeness by incorporating additional excitation sources (e.g. rolling bearings) and enabling stronger coupling via time-domain simulations. This would also help address residual discrepancies between simulations and test bench observations.

Another possible development involves integrating the electric motor control loop, as potential dynamic instabilities linked to the control architecture must be anticipated.

Finally, current gear meshing excitations were computed without considering electric engine -induced torque ripple. Extending the model to capture this interaction would represent a significant advance toward a more comprehensive and efficient simulation framework.

Authors contact:

Dr. Jessica NEUFOND, jessica.neufond@vibratec.fr

Adrien PARPINEL, adrien.parpinel@vibratec.fr

Lionel DUVERMY, lionel.duvermy@vibratec.fr

7. ACKNOWLEDGMENTS

The authors thank all the participants of the TURBO-LAB project, as well as its contributors, DGAC via FRANCE 2030 investment plan organization, the European Union and SAFRAN Group. The authors also thank AKIRA Technologies Corporation for their implication and partnership in this project.

REFERENCES

1. Dupont, J., Bouvet, P., Wojtowicki, J., "Simulation of the Airborne and Structure-Borne Noise of Electric Powertrain: Validation of the Simulation Methodology", *SAE Technical Paper 2013-01-2005*, 2013, doi:10.4271/2013-01-2005

2. Neufond, J., "Comportement dynamique et vibroacoustique des trains planétaires*", PhD thesis report,* Ecole Centrale de Lyon, 2020

3. Harris, SL., "Dynamic loads on the teeth of spur gears.", *IMechE Proceedings*, 172: 87–112, 1958

4. Mar Welbourn DB., “Fundamental knowledge of gear noise – a survey.”, *Conf Noise Vibrat Engines Trans Proceedings*, C177/79: 9–29, 1979

5. Van Binsbergen, D., Valavi, M., Nejad, A.R. et al, “Effect of generator torque ripple optimization on a geared wind turbine drivetrain.”, *Forsch Ingenieurwes* 87, 197–205, 2023, https://doi.org/10.1007/s10010-023-00624-3

6. Carbonelli, A., “Caractérisation vibro-acoustique d’une cascade de distribution poids lourd.”, *PhD thesis report,* Ecole Centrale de Lyon, 2012

7. Parpinel, A., Neufond, J., Duvermy, L., “TURBOLAB – test rig demonstrator for electromagnetic and gear mesh loads”, 50th European Rotorcraft Forum Proceedings, paper number 169, Marseille, September 2024